FULL PAPER *Pathology*

Demonstration of the Clathrin- and Caveolin-Mediated Endocytosis at the Maternal–Fetal Barrier in Mouse Placenta after Intravenous Administration of Gold Nanoparticles

Kasem RATTANAPINYOPITUK[1,2], Akinori SHIMADA[3]*, Takehito MORITA[1,2], Masashi SAKURAI[1,2], Atsushi ASANO[4], Tatsuya HASEGAWA[5], Kenichiro INOUE[6] and Hirohisa TAKANO[7]

[1]*Department of Veterinary Pathology, Tottori University, 4–101 Koyama Minami, Tottori 680–8553, Japan*
[2]*The United Graduate School of Veterinary Science, Yamaguchi University, 1667–1 Yoshida, Yamaguchi 753–8515, Japan*
[3]*Laboratory of Pathology, School of Life and Environmental Science, Azabu University, 1–17–71 Fuchinobe, Sagamihara-shi, Kanagawa 252–5201, Japan*
[4]*Department of Veterinary Biochemistry, Tottori University, 4–101 Koyama Minami, Tottori 680–8553, Japan*
[5]*Department of Environmental Biochemistry, Yamanashi Institute of Environmental Sciences, 5597-1 Fujiyoshida, Yamanashi 403–0005, Japan*
[6]*Basic Medical Research Center, International University of Health and Welfare, 2600–1 Kitakanamura, Ootawara-shi, Tochigi 324–8501, Japan*
[7]*Department of Environmental Engineering, Kyoto University Graduate School of Engineering, Kyoto Daigaku Katsura, Saikyo-ku, Kyoto 615–8530, Japan*

(Received 15 October 2013/Accepted 6 November 2013/Published online in J-STAGE 20 November 2013)

ABSTRACT. Exposure to nanoparticles during pregnancy is a public concern, because nanoparticles may pass from the mother to the fetus across the placenta. The purpose of this study was to determine the possible translocation pathway of gold nanoparticles across the maternal–fetal barrier as well as the toxicity of intravenously administered gold nanoparticles to the placenta and fetus. Pregnant ICR mice were intravenously injected with 0.01% of 20- and 50-nm gold nanoparticle solutions on the 16th and 17th days of gestation. There was no sign of toxic damage to the placentas as well as maternal and fetal organs of the mice treated with 20- and 50-nm gold nanoparticles. ICP-MS analysis demonstrated significant amounts of gold deposited in the maternal livers and placentas, but no detectable level of gold in the fetal organs. However, electron microscopy demonstrated an increase of endocytic vesicles in the cytoplasm of syncytiotrophoblasts and fetal endothelial cells in the maternal–fetal barrier of mice treated with gold nanoparticles. Clathrin immunohistochemistry and immunoblotting showed increased immunoreactivity of clathrin protein in the placental tissues of mice treated with 20- and 50-nm gold nanoparticles; clathrin immunopositivity was observed in syncytiotrophoblasts and fetal endothelial cells. In contrast, caveolin-1 immunopositivity was observed exclusively in the fetal endothelium. These findings suggested that intravenous administration of gold nanoparticles may upregulate clathrin- and caveolin-mediated endocytosis at the maternal–fetal barrier in mouse placenta.
KEY WORDS: caveolin, clathrin, endocytosis, gold nanoparticles, placenta.

doi: 10.1292/jvms.13-0512; *J. Vet. Med. Sci.* 76(3): 377–387, 2014

The development of nanotechnology has resulted in rapid expansion of the use of nanoparticles in various categories, e.g., food, cosmetic, electronic, medical and pharmaceutical industries [15, 31, 32, 36, 39, 40]. Because nanoparticles have properties, such as an extremely small size (less than 100 nm in diameter), high surface area per mass ratio and high potential chemical activities, adverse health effects from the daily application of nanoparticles have been seriously considered [5, 9, 10, 24, 32, 34]. The fetus is known to be susceptible to various toxic substances [1, 15, 39]. Therefore, there is high concern regarding exposure to exogenous substances, including nanosized materials, for pregnant women [12, 32, 39].

The placenta is the organ that connects the maternal and fetal circulation. Oxygen and nutrient exchanges between the mother and fetus occur in the maternal–fetal barrier at the labyrinthine zone of the placenta [4, 11, 13, 14, 37]. In addition, toxic substances can also transfer across the maternal–fetal barrier. Therefore, the placenta is a critical site for fetal intoxication [10, 12, 32]. Placental structure differs among animals. Human and rodent have the same type of placenta, hemochorial type. There are, however, some differences in the placental structures between humans and rodents [12, 39]. Human maternal–fetal barrier consists of one trophoblastic layer (syncytiotrophoblast layer) on the maternal side with underlying discontinuous cytotrophoblastic layer, basement membrane and fetal endothelial cells on the fetal side. In contrast, mouse maternal–fetal barrier has 3 trophoblastic layers on the maternal side that connect each layer with tight gap junction with underlying fetal endothelial cells on the

*CORRESPONDENCE TO: SHIMADA, A., Laboratory of Pathology, School of Life and Environmental Science, Azabu University, 1–17–71 Fuchinobe, Sagamihara-shi, Kanagawa 252–5201, Japan.
e-mail: a-shimada@azabu-u.ac.jp

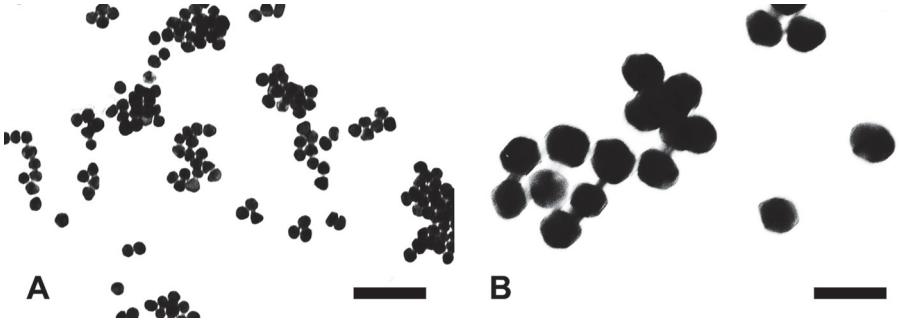

Fig. 1. Electron micrographs of 20-nm (A) and 50-nm (B) gold nanoparticles show electron-dense, spherical, uniform and individual or slightly agglomerated appearance. Bar=100 nm.

Table 1. Gold contents in the tissues measured by ICP-MS

Group		Gold content (μg/g dry tissue)		
		Maternal liver	Placenta	Fetal liver
Control	(n=2)	0.2 ± 0.07	ND	ND
20-nm gold NPs	(n=3)	640.3 ± 171.80[a)]	1.3 ± 0.61	ND
50-nm gold NPs	(n=3)	99.2 ± 2.75[b)]	1.0 ± 0.78	ND

Values are the mean ± standard error. a) Significantly different between the control and 20 nm gold NPs injected mice, $P<0.05$. b) Significantly different between 20-nm gold NPs injected mice and 50-nm gold NPs injected mice, $P<0.05$. NPs=Nanoparticles. ND=Not detected.

fetal side [13–15, 32]. Despite such anatomical differences, rodent placentas are regarded as advantage of the ethical reason and of similarities in placental functions and have been used to study the function of human placenta in every stage of pregnancy [12, 22, 32, 39].

The mechanisms of placental exchange for several endogenous substances include passive and facilitated diffusion, via transtrophoblastic channels and active transport, e.g., via endocytosis [4, 15, 32]. Endocytosis may be an important mechanism for certain types of nanoparticle translocation across the maternal–fetal barrier [4, 15, 32]. Macropinocytosis and classical clathrin-dependent, non-classical clathrin-independent (caveolae-dependent) or clathrin- and caveolae-independent endocytosis are further proposed as subtypes of endocytosis [6, 18, 21, 24]. Clathrin, a major protein of clathrin-coated endocytic vesicles, and caveolin-1, a major protein of the caveolae structure [22], are expressed in trophoblasts and endothelial cells of the human placenta during physiological condition. However, information about the expression of clathrin and caveolin-1 in the placental tissue during nanoparticle exposure remains unclear. Therefore, the present study aimed to examine the clathrin- and caveolin-mediated endocytosis after intravenous administration of gold nanoparticles in mouse placenta.

MATERIALS AND METHODS

Animals: Sixteen pregnant ICR mice at gestation day 16 (GD16) (15–17 weeks old, 55–75 g) were obtained from CLEA Japan Inc. (Tokyo, Japan). Commercial diet CE-2 (CLEA Japan Inc.) and tap water were given *ad libitum* throughout the experiment. The mice were housed at approximately 25°C and 55–70% relative humidity under a 12-hr light/dark cycle. The experiments were approved by the Institutional Animal Care and Use Committee, and all procedures were conducted according to the Tottori University guidlines for animal welfare.

Particles morphology of gold nanoparticles: The experiment employed 20- and 50-nm colloidal gold solutions (mean diameters of 19.6 nm and 49.3 nm respectively, according to the manufacturer's information; BB International, Cardiff, U.K.). The morphology of the gold nanoparticles was examined by transmission electron microscopy (TEM-100CX; Japan Electron Optical Laboratory, Tokyo, Japan). The 20-nm and 50-nm colloidal gold solutions contained electron-dense, spherical, uniform and individual or slightly agglomerated particles (Fig. 1).

Experimental protocol: At GD16, pregnant ICR mice were intravenously injected with 0.5 m*l* of saline solution (control, n=4), 20-nm or 50-nm colloidal gold solutions through the tail vein (n=6 per treatment). At 24 hr after the first injection, the pregnant mice (GD17) were intravenously injected with the same solutions as the previous injections. At 24 hr after the second injection, the pregnant mice (GD18) were sacrificed by performing exsanguination under deep anesthesia induced by the intraperitoneal injection of sodium pentobarbital. Then, tissue samples were collected.

Sampling for maternal organs, plancentas and fetal organs: Maternal livers, placentas and fetal livers were collected from the pregnant mice and fetuses after gross examination. The samples were used for histopathological, immunohistochemical, autometallography (AMG) and

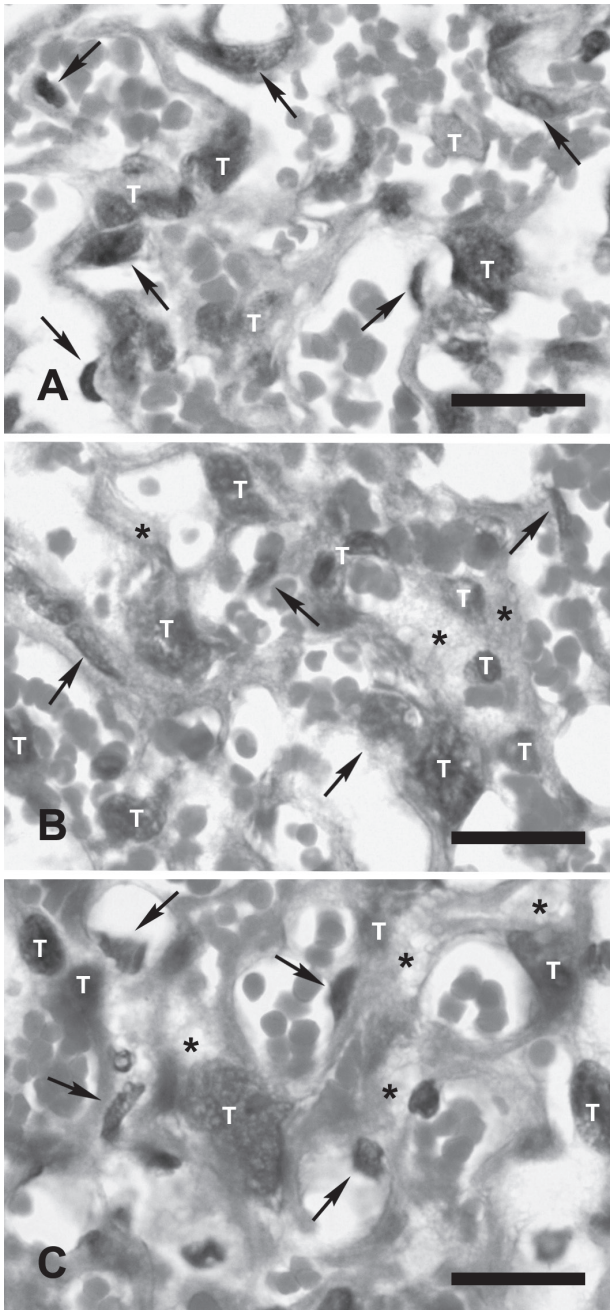

Fig. 2. Maternal–fetal barrier in the labyrinthine zone of the placentas from control mice (A) and from mice injected with 20-nm (B) and 50-nm gold nanoparticles (C). No severe histopathological lesions are observed. Mild swelling of the cytoplasm (asterisks) of syncytiotrophoblastic cells (T) and endothelial cells (arrows) are observed at the maternal–fetal barrier from mice injected with 20- and 50-nm gold nanoparticles. Bar=50 μm.

transmission electron microscopy examinations.

Inductively coupled plasma-mass spectroscopy (ICP-MS): Maternal livers, placentas and fetal livers (0.1 g of each tissue; n=2 from the control or n=3 from mice that were injected with gold nanoparticles) were digested with 2 m*l* of aqua regia. After digestion, the inorganic residues were dissolved in 5 m*l* of 0.05 N HCl and ultrasonicated for 20 min, and the samples were then analyzed by performing inductively coupled plasma-mass spectroscopy (ICP-MS) (HP 4500; Agilent Technologies, Santa Clara, CA, U.S.A.). Detection and quantification limits for gold were 0.5 *n*g/m*l* and 1 *n*g/m*l*, respectively [35].

Histopathology: Maternal livers, placentas and fetal livers were fixed in 10% neutral-buffered formalin. The formalin-fixed tissues were processed using routine pathological methods and embedded in paraffin blocks. Paraffin-embedded sections (4-μm-thick) were cut for hematoxylin and eosin staining, immunohistochemistry and AMG. Histopathological examination was performed by 2 pathologists in a blind manner under a light microscope.

Autometallography (AMG): Paraffin-embedded sections of placenta, maternal liver and fetal liver were used for AMG staining [7, 8]. The sections were developed in a physical developer consisting of 50% gum arabic, 50% citrate buffer, 5.6% hydroquinone and 17% silver nitrate. The reaction was conducted in a water bath at 26°C for 1 hr in the dark. Excessive silver residue was removed with a 5% sodium thiosulfate solution for 10 min. Next, the sections were counterstained with hematoxylin. A positive result was demonstrated as small black silver grains inside the cells of interest.

Immunohistochemistry: Paraffin-embedded sections of the placentas were used for the immunohistochemical detection of clathrin, caveolin, interleukin (IL)-6, tumor necrotic factor (TNF)-α, dimeric copper- and zinc-containing superoxide dismutase (Cu/Zn SOD), inducible nitric oxide synthase (iNOS) and caspase-3. For antigen retrieval, the sections were treated with citrate buffer (pH 5.4) and then microwaved. Endogenous peroxidase activity was quenched with 3% H_2O_2 at room temperature for 30 min. The slides were then blocked with 10% normal goat serum (for the detection of clathrin, caveolin-1, IL-6, TNF-α, Cu/Zn SOD, iNOS and caspase-3) or 10% bovine serum albumin (for the detection of IL-6) for 5 min in a microwave. Next, the sections were incubated with primary antibodies at 4°C overnight (anti-clathrin heavy chain: Abcam, Cambridge, MA, U.S.A. 1:7,000 dilution; anti-caveolin-1: Santa Cruz Biotechnology, Santa Cruz, CA, U.S.A. 1:1,500 dilution; anti-IL-6: Santa Cruz Biotechnology 1:200 dilution; TNF-α: Monosan, Uden, the Netherlands, 1:15 dilution; anti-Cu/Zn SOD: Stressgen Bioreagents, Victoria, Canada, 1:200 dilution; anti-iNOS: BD Transduction Laboratories, Lexington, KY, U.S.A. 1:125 dilution; and anti-caspase-3: Promega, Madison, WI, U.S.A 1:250) or an equivalent amount of phosphate-buffered saline as a negative control. A labeled streptavidin biotin kit (Dako, Glostrup, Denmark) was used to detect immunoreaction complexes in the avidin–biotin complex assay. Positive immunoreactions appeared as brown staining with 3,3′-diaminobenzidine tetrahydrochloride (DAB). The sections were counterstained with hematoxylin and observed by light microscopy in 4 randomly selected lesions at 100× magnification. Positive immunolabeling areas

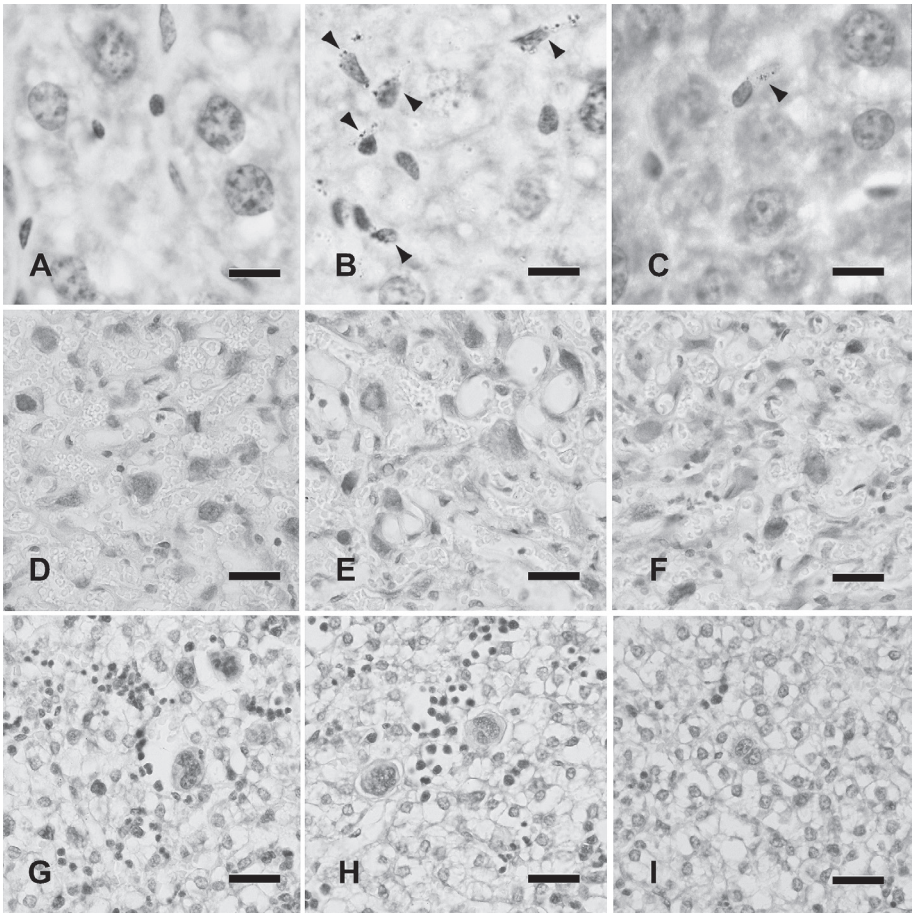

Fig. 3. Autometallographic-enhanced gold nanoparticles in maternal livers (A–C), placentas (D–F) and fetal livers (G–I) of control mice (A, D and G), mice intravenously injected with 20-nm gold nanoparticles (B, E and H) and 50-nm gold nanoparticles (C, F and I). Gold nanoparticles are demonstrated exclusively in the maternal livers from mice injected with 20- and 50-nm gold nanoparticles. The deposition of gold nanoparticles is shown in Kupffer cells (arrowheads) (B and C). Autometallography shows negative staining in all tissues from the control mice (A, D and G), placentas (E and F) and fetal livers (H and I) from mice injected with 20- and 50-nm gold nanoparticles. A–C; bar=10 μm; D–I; bar=25 μm.

were analyzed in 5 randomly selected areas from each group by using Image-Pro Plus 6.1 software (MediaCybernetics, Inc., Silver Spring, MD, U.S.A.).

Double immunofluorescence: The sections were placed in citrated buffer solution (pH=5.4), microwaved and then treated with proteinase K for 15 min for antigen retrieval. Next, the sections were incubated with normal goat serum for 5 min in a microwave. After incubation with normal goat serum, the sections were applied to the primary antibodies against clathrin (1:500 dilution) or caveolin-1 (1:350 dilution) overnight at 4°C and then incubated with Alexa Fluor 488-conjugated secondary antibody (1:200 dilution) for 1 hr at room temperature. Then, the sections were reacted with primary antibody against cytokeratin (Dako, 1:100 dilution) overnight at 4°C and then incubated with Alexa Fluor 555-conjugated secondary antibody (1:300 dilution) for 30 min at room temperature. Thereafter, the sections were mounted in plain 80% Tris-buffered glycerol. Analyses were performed with a confocal imaging system (AX-70, Olympus Laboratory, Tokyo, Japan).

Electron microscopy: Half of the longitudinal sections from the placenta were cut into cubes measuring 1–2 mm^3. Next, tissues were fixed in glutaraldehyde for 3 hr at 4°C, rinsed in 0.1 M phosphate buffer (pH 7.4), postfixed with 1% osmium tetroxide for 1 hr, dehydrated in alcohol and embedded in epoxy resin. The areas of interest were selected for electron microscopy examination from 1% toluidine-stained semi-thin (1-μm-thick) sections and subsequently cut into ultra-thin (70-nm-thick) sections. After staining with uranyl acetate and lead citrate, ultra-thin sections were examined using a transmission electron microscope (TEM-100CX; Japan Electron Optical Laboratory, Tokyo, Japan).

Western blot analysis: Approximately 100 mg of placental tissue (n=4 per group) was harvested and processed in lysis

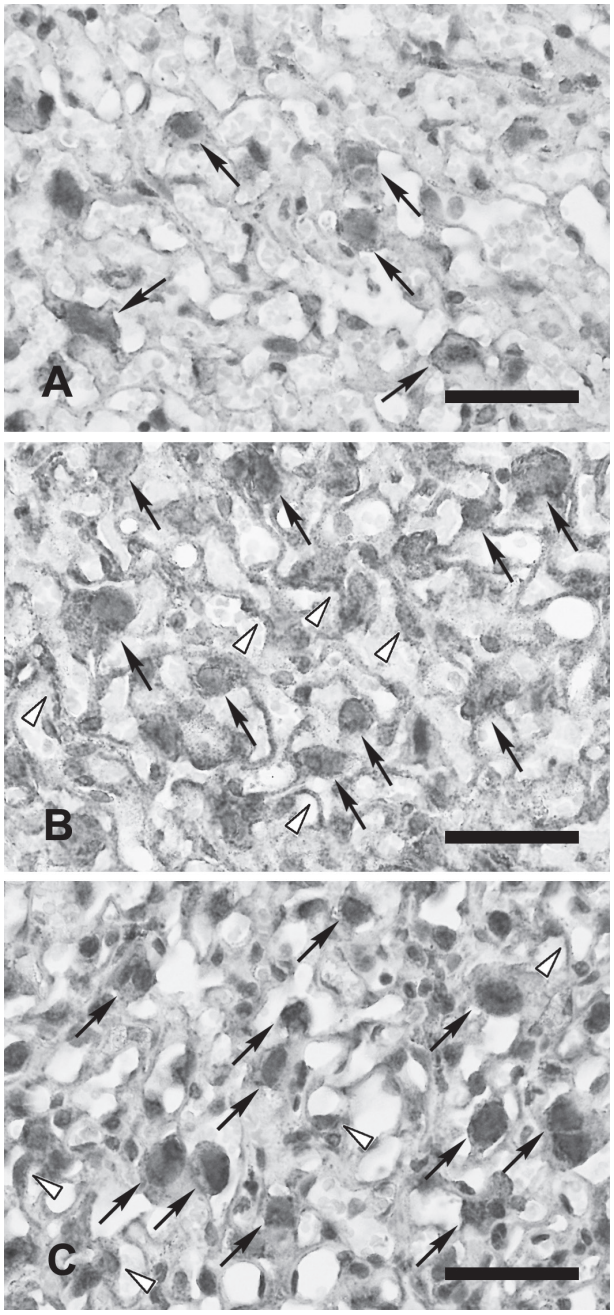

Fig. 4. Clathrin immunohistochemistry showing intense positivity in the cytoplasm of trophoblastic cells (arrows) and endothelial cells (white arrowheads) in the maternal–fetal barrier in the labyrinthine zone of placentas from mice injected with 20-nm (B) and 50-nm (C) gold nanoparticles. Weak positivity is shown in the cytoplasm of trophoblastic cells (arrows) and fetal endothelial cells (white arrowheads) in the maternal–fetal barrier from a control mouse (A). Counterstained with hematoxylin. Bars=100 μm.

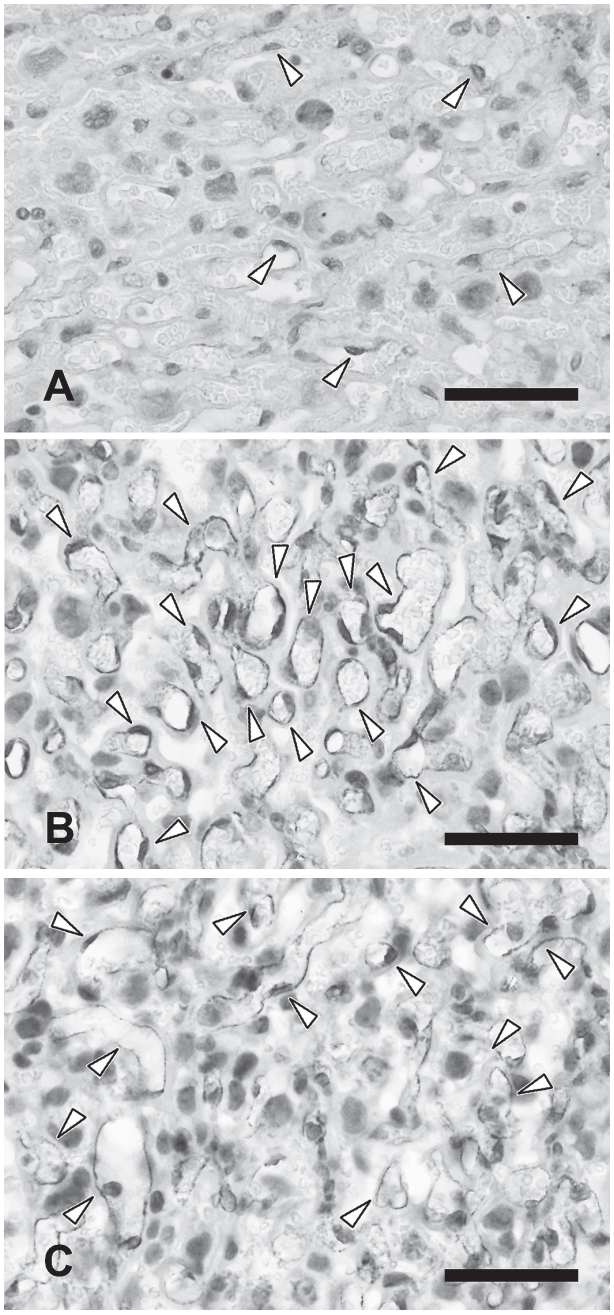

Fig. 5. Caveolin-1 immunohistochemistry showing immunopositivity in the cytoplasm of fetal endothelial cells at the maternal–fetal barrier in the labyrinthine zone of the placentas (white arrowheads) from mice injected with 20-nm (B) and 50-nm (C) gold nanoparticles. Weak positivity is shown in the cytoplasm of fetal endothelial cells in the maternal–fetal barrier from a control mouse (A). Counterstained with hematoxylin. Bars=100 μm.

buffer (Roche, Basel, Switzerland) to extract protein. Tissue lysates were clarified by centrifugation at 14,000 rpm for 10 min, and the protein content of the supernatant was determined. Lysate supernatants were diluted 1:1 with 2× electrophoresis sample buffer (1× sample buffer=125 mM Tris–HCl, pH 6.8, 2% sodium dodecyl sulfate [SDS], 5% glycerol, 0.003% bromophenol blue and 1% β-mercaptoethanol), and

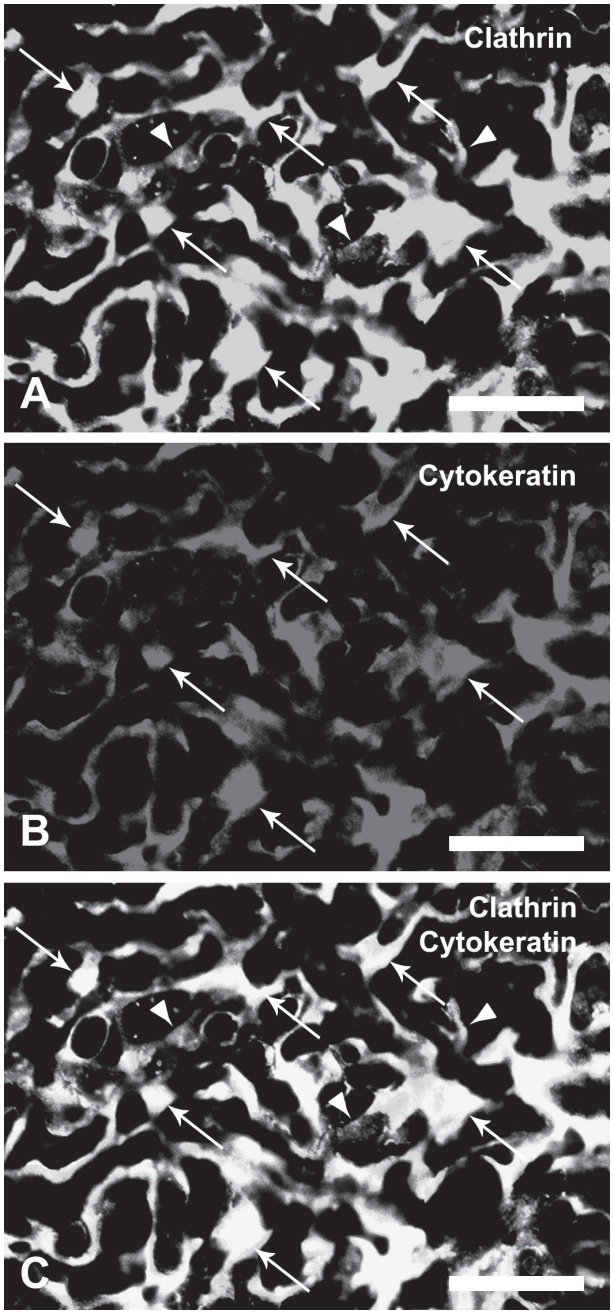

Fig. 6. Double immunofluorescence of clathrin and cytokeratin proteins in the labyrinthine zone of mice placenta. Double immunolabeling by using antibodies against clathrin as shown by Alexa 488 (green) (A) and cytokeratin as shown by Alexa 555 (red) (B). Merged image with the 2 fluorophores (C). The syncytiotrophoblast layer (white arrows) and fetal vascular wall are strongly labeled with clathrin (white arrowheads) (A). The syncytiotrophoblast layer is exclusively labeled with cytokeratin (white arrows) (B). Co-expression of clathrin and cytokeratin (yellowish) is shown in the syncytiotrophoblast layer (white arrows) (C). Bars=100 μm.

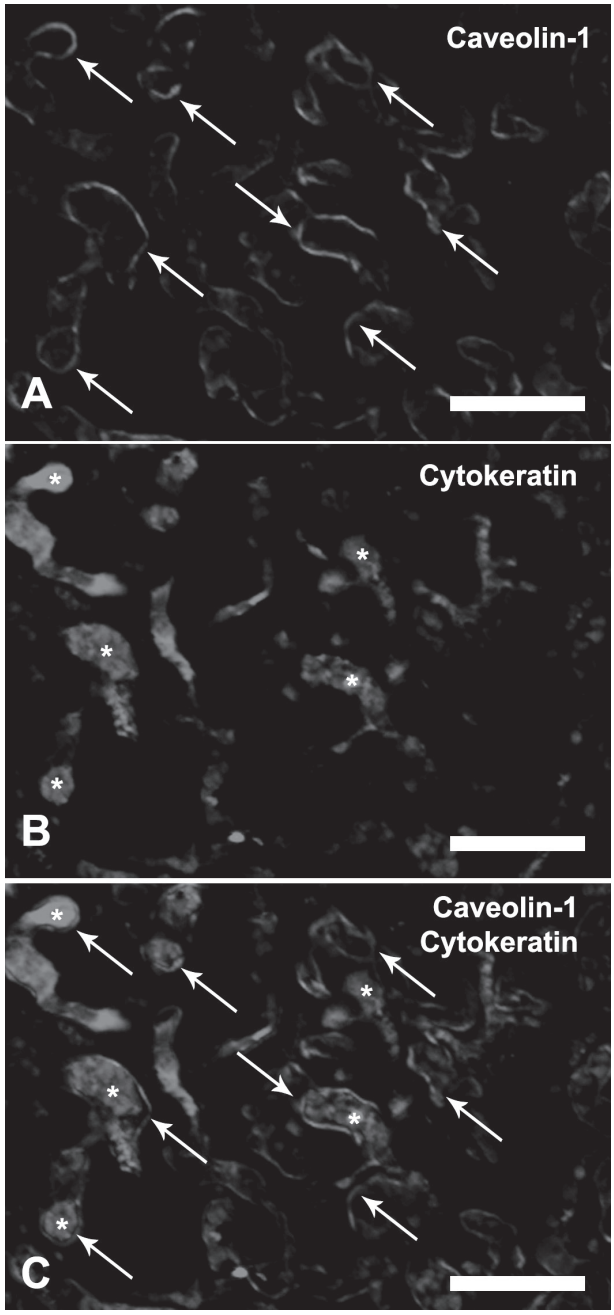

Fig. 7. Double immunofluorescence of caveolin-1 and cytokeratin proteins in the labyrinthine zone of mice placenta. Double immunolabeling by using antibodies against caveolin-1 as shown by Alexa 488 (green) (A) and cytokeratin as shown by Alexa 555 (red) (B). Merged image with the 2 fluorophores (C). The fetal vascular wall is exclusively labeled with caveolin-1 (white arrows) (A). The syncytiotrophoblast layer is labeled with cytokeratin (white asterisks) (B). Co-expression of caveolin-1 and cytokeratin is not shown in the labyrinthine zone of the placenta. Bars=100 μm.

aliquots equivalent to 20 μg of total protein per sample were resolved in a 15% SDS/polyacrylamide gel. The gels were electroblotted onto a polyvinylidene difluoride membrane (BioRad, Hertfordshire, U.K.), and the membrane was

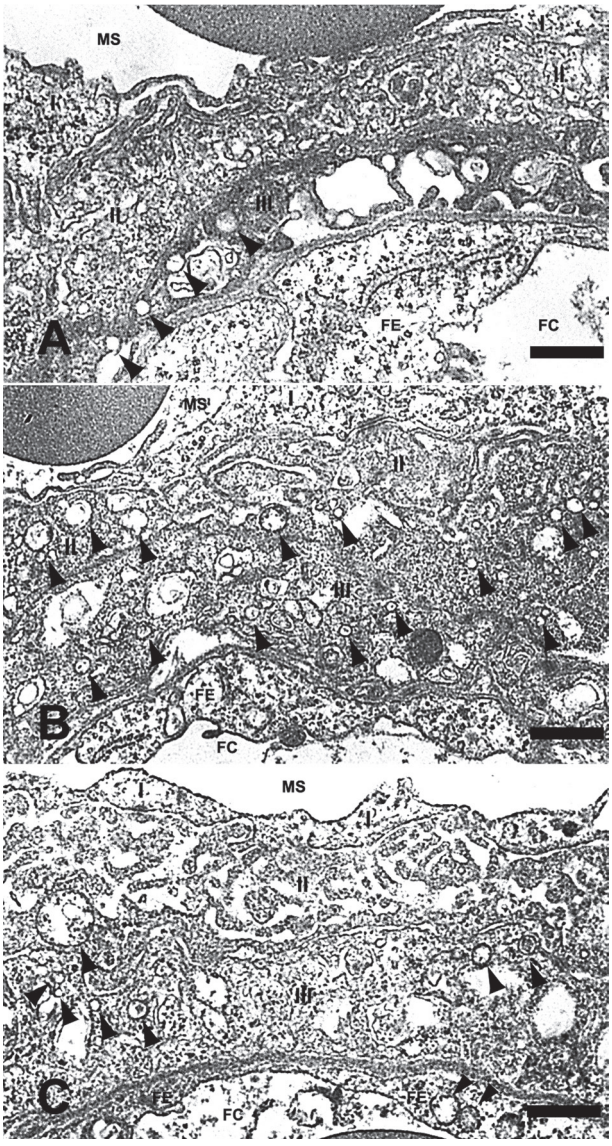

Fig. 8. Transmission electron micrographs of maternal–fetal barrier in the labyrinthine zone of the placentas. The placenta from a control mouse consists of 3 syncytiotrophoblast layers with underlying fetal endothelial cells. Numerous microplicae and infolding with a few of vesicle-like structures (arrowheads) are shown in the cytoplasm of syncytiotrophoblast layers II and III in the maternal–fetal barrier from a control mouse (A). Enlargement of the cytoplasm of syncytiotrophoblast layer I, II, III and fetal endothelial cells with an increase in the number of vesicle-like structures (arrowheads) is shown in the maternal–fetal barrier from mice injected with 20-nm (B) and 50-nm (C) gold nanoparticles. Bar=0.5 μm. MS=maternal blood sinus, I=syncytiotrophoblast layer I, II=syncytiotrophoblast layer II, III=syncytiotrophoblast layer III, FE=fetal endothelial cell, FC=fetal capillary.

probed with the primary antibodies, rabbit anti-clathrin heavy chain (1:1,000 dilution) or rabbit anti-caveolin-1 (1:1,000 dilution). After overnight incubation at 4°C, the membrane was washed and probed with the secondary antibody, which was an anti-rabbit horse radish-peroxidase-conjugated IgG. After incubation for 1 hr, the membrane was washed. The immunoblot procedure was performed using the chemiluminescence detection reagent (Luminata^{TM} Forte Western HRP Substrate, Millipore, Billerica, MA, U.S.A.) according to the manufacturer's protocol. The bands on the clarified blots were measured with an image analysis system (Image-Pro Plus 6.1, MediaCybernetics, Inc., Silver Spring, MD, U.S.A.), and the digital numbers that were obtained were integrated density values of the intensity of each band.

In situ apoptosis detection (TUNEL assay): Paraffin-embedded sections of placenta were treated with proteinase K at room temperature. Then, the sections were inactivated for endogenous peroxidase by applying 3% H_2O_2 for 5 min. After washing, the labeling reaction mixture (consisting of TdT enzyme and labeling safe buffer, *in situ* apoptosis detection kit: Takara Bio Inc., Otsu, Japan) was applied to the sections, and they were incubated in a 37°C humidified chamber for 70 min. Following this, the sections were treated with Anti-FITC HRP conjugate (Takara Bio Inc.) and incubated at 37°C for 30 min. After coloring with DAB, the sections were counterstained with 3% methyl green and observed under a light microscope.

Statistical analysis: All of the data were expressed as the mean ± standard error. Statistical significance was determined by performing the Mann-Whitney's U-test or the Student's *t*-test for 2-group comparisons. For all comparisons, *P* values less than 5% ($P<0.05$) were considered statistically significant.

RESULTS

ICP–MS: Gold was detected in the maternal livers and placentas from mice injected with 20- and 50-nm gold nanoparticles (Table 1). The level of gold in both maternal livers and placentas from mice injected with 20-nm gold nanoparticles was significantly higher than the level of gold from mice injected with 50-nm gold nanoparticles. Gold was not detected in maternal livers and placentas from control mice and fetal livers from the control mice and the mice injected with 20- and 50-nm gold nanoparticles.

Histopathology: Placental tissues from mice injected with 20- and 50-nm gold nanoparticles demonstrated no significant pathological changes at the maternal–fetal barrier in the labyrinthine zone of the placentas compared to the control mice (Fig. 2). Only mild swelling of the cytoplasm of syncytiotrophoblastic cells and fetal endothelial cells in the maternal–fetal barrier from mice injected with gold nanoparticles was occasionally observed (Fig. 2B and 2C).

No pathological lesions were found in other maternal and fetal organs from the control mice and the mice injected with 20- and 50-nm gold nanoparticles.

Autometallography: Silver-enhanced gold nanoparticles were detected in Kupffer cells in the maternal livers of mice injected with 20- and 50-nm gold nanoparticles (Fig. 3B and 3C). Gold nanoparticles were not detected by using the AMG method in the placentas, maternal livers and fetal livers from the control mice and placentas and fetal livers from the mice

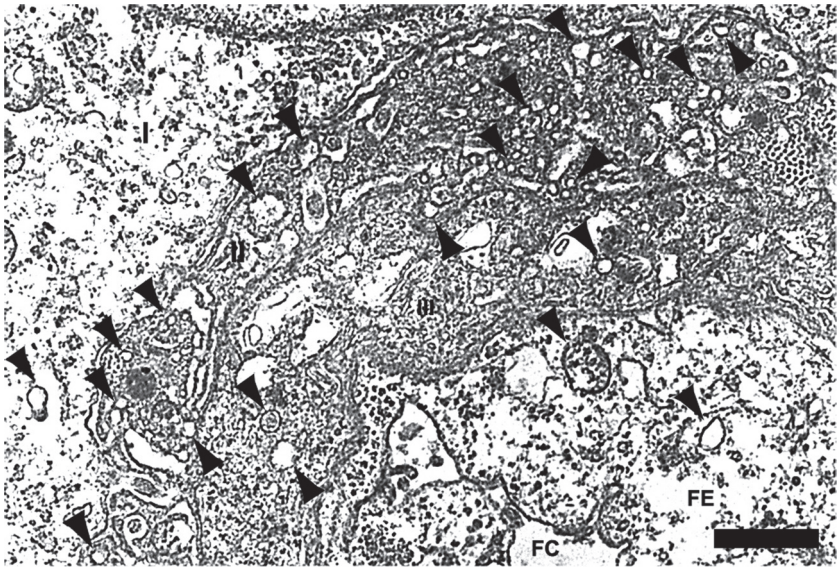

Fig. 9. Transmission electron micrograph of the maternal–fetal barrier in the labyrinthine zone of the placenta from mouse injected with 20-nm gold nanoparticles demonstrating an increase in the number of vesicle-like structures (arrowheads) in the cytoplasm of syncytiotrophoblast layers I, II, III, and fetal endothelial cells. Bar=0.5 μm. I=syncytiotrophoblast layer I, II=syncytiotrophoblast layer II, III=syncytiotrophoblast layer III, FE=fetal endothelial cell, FC=fetal capillary.

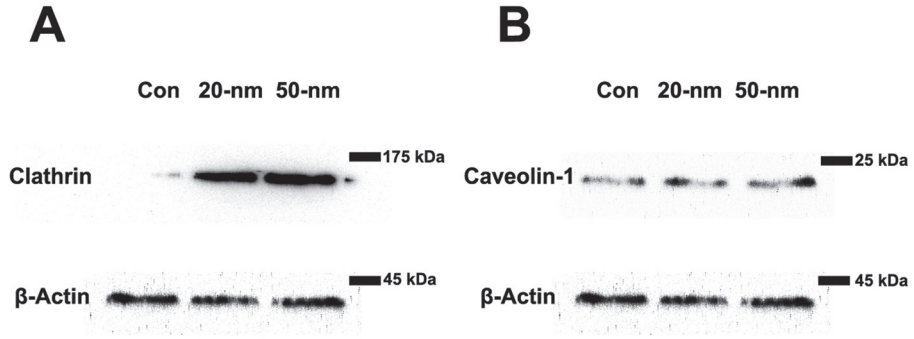

Fig. 10. Western blotting demonstrates clathrin and caveolin-1 protein expression in the placental tissues from pregnant mice. The intensity of clathrin protein band (171 kDa) of placental tissue lysates from control mice is less than the bands of tissue lysates from mice injected with 20- and 50-nm gold nanoparticles (A). The intensity of caveolin-1 protein bands is not different between the control mice and the mice treated with 20- and 50-nm gold nanoparticles (B).

injected with 20- and 50-nm gold nanoparticles (Fig. 3).

Immunohistochemistry: Clathrin immunohistochemistry demonstrated positive reaction in syncytiotrophoblastic cells and fetal endothelial cells (Fig. 4). Weak positivity was observed in syncytiotrophoblastic cells and fetal endothelial cells at the maternal–fetal barrier from the control mice (Fig. 4A) compared to mice injected with gold nanoparticles (Fig. 4B and 4C). The image analysis of clathrin immunopositivity showed higher intensity in the placental tissues from mice injected with gold nanoparticles. No significant differences were observed between clathrin immunoreactivity in the placental tissues from mice injected with 20- and 50-nm gold nanoparticles as seen by using image analysis (Table 2).

Caveolin-1 immunoreactivity was detected exclusively in the cytoplasm of fetal endothelial cells at the maternal–fetal barrier in the labyrinthine zone of the placentas (Fig. 5). The positivity of caveolin-1 immunolabeling was lesser in the placental tissues from the control mice (Fig. 5A) compared to mice injected with gold nanoparticles (Fig. 5B and 5C). The image analysis of caveolin-1 immunolabeling showed higher intensity in the placental tissues from mice injected with gold nanoparticles. No significant differences were observed between caveolin-1 immunoreactivity in the placental tissues from mice injected with 20- and 50-nm gold

Table 2. Positive immunolabeling area in the labyrinthine zone of placentas

Group	% Positive area[a)]	
	Anti-caveolin-1	Anti-clathrin
Control	0.28 ± 0.179	2.73 ± 0.430
20-nm gold NPs	3.57 ± 0.718[b)]	12.04 ± 1.495[b)]
50-nm gold NPs	2.57 ± 0.926[b)]	9.10 ± 1.618[b)]

Values are the mean ± standard error. a) Positive area (%) of 94,850 μm^2 of 4-μm-thick paraffin sections. b) Significantly different from the control group, $P<0.05$. NPs=Nanoparticles.

Table 3. Integrated density values of the immunoblot band intensity using the image analysis system

Protein	Density of immunoblot band intensity (optical density unit)		
	Control (n=3)	20-nm gold NPs (n=3)	50-nm gold NPs (n=3)
Clathrin	0.20 ± 0.062	1.05 ± 0.029[a)]	1.06 ± 0.010[a)]
Caveolin-1	1.46 ± 0.167	1.36 ± 0.224	1.55 ± 0.095

Values are the mean ± standard error. a) Significantly different from the control group, $P<0.05$. NPs=Nanoparticles.

nanoparticles as seen by using image analysis (Table 2).

There were occasional positive findings in IL-6, TNF-α, Cu/Zn SOD and iNOS immunolabeling in the cytoplasm of syncytiotrophoblasts and fetal endothelial cells in the maternal–fetal barrier. No difference in the intensity and distribution of IL-6, TNF-α, Cu/Zn SOD and iNOS immunolabeling between the control mice and the mice injected with 20- and 50-nm gold nanoparticles was observed (data not shown). No positivity in caspase-3 immunolabeling was detected in the maternal–fetal barrier from the control mice and the mice injected with 20- and 50-nm gold nanoparticles (data not shown).

Double immunofluorescence: Positive clathrin immunoreactivity was demonstrated in the syncytiotrophoblast layer and fetal vascular endothelium (Fig. 6A). The colocalization of clathrin and cytokeratin was observed in the syncytiotrophoblast layer (Fig. 6C). In contrast, caveolin-1 immunoreactivity revealed strong immunoreactivity exclusively in fetal vascular endothelial cells (Fig. 7A). The colocalization of caveolin-1 and cytokeratin was not observed in the labyrinthine zone of the placentas (Fig. 7C).

Electron microscopy: The maternal–fetal barrier in the labyrinthine zone of the placentas from the control mice consisted of 3 layers of syncytiotrophoblastic cells (syncytiotrophoblast layers I, II and III) with underlying fetal endothelial cells. Electron microscopy demonstrated no signs of cell/tissue damage in the placenta from the mice treated with gold nanoparticles. Numerous microplicae and infolding with a few vesicle-like structures were observed in the cytoplasm of syncytiotrophoblast layers II and III in the maternal–fetal barrier from the control mice (Fig. 8A). Moderate enlargement with an increase in the number of vesicle-like structures was observed in the cytoplasm of syncytiotrophoblast layers II and III in the maternal–fetal barrier from mice injected with 20- and 50-nm gold nanoparticles (Figs. 8B, 8C and 9). An increase in the number of vesicle-like structures was also shown in the endothelial cells in the maternal–fetal barrier from mice injected with 20- and 50-nm gold nanoparticles compared to the control mice (Figs. 8C and 9).

Western blot analysis: Immunoblotting of tissue lysates from placentas of mice injected with 20- and 50-nm gold nanoparticle solutions demonstrated a 171-kDa band of clathrin protein. The positive band from the control mice was less intense compared to positive bands from mice injected with gold nanoparticles (Fig. 10A). The integrated density values of the intensity of bands of tissue lysates from mice injected with gold nanoparticles were significantly greater than those of the control mice (Table 3).

A 22-kDa band representing caveolin-1 was observed in the placental tissue lysates. The positive bands showed no difference in intensity in the placental lysates from the control mice and the mice injected with gold nanoparticles (Fig. 10B). The integrated density values of the intensity of bands of the tissue lysates were not significantly different between all groups (Table 3).

In situ apoptosis detection (TUNEL assay): The TUNEL assay showed negative results in the labyrinthine zone of the placentas of control, 20- and 50-nm gold nanoparticle injected mice (data not shown).

DISCUSSION

At present, the risk of exposure to nanosized materials in pregnancy is increasing. However, there are only a few studies on the translocation pathway of nanoparticles across the maternal–fetal barrier (placental barrier) [5, 9, 15]. The present study aims to determine the possible translocation mechanism of gold nanoparticles across the maternal–fetal barrier of mice.

ICP-MS analysis demonstrated a significant amount of gold deposited in the maternal livers and placentas, but no detectable level of gold in the fetal organs. Although AMG staining also showed the dominant accumulation of gold nanoparticles in Kupffer cells in the livers of the pregnant mice, no AMG positive findings were observed in the fetuses after intravenous administration. The liver is a major organ for the elimination of circulating nanoparticles [29]. A previous study also reported that gold nanoparticles are primarily phagocytized by Kupffer cells and that almost of the administered nanoparticles present in the liver after intravenous administration in rodents [2, 29, 30, 33].

No pathological changes were observed in the placentas, maternal organs and fetal organs from mice treated with 20-nm and 50-nm gold nanoparticle solutions, suggesting that gold nanoparticles would not be harmful to pregnant mice and their placentas at the doses that we used. Previous *in vitro* and *in vivo* studies also reported that various sizes and doses of gold nanoparticles showed no obvious toxicity to mice and rats [17, 31, 33].

Previous studies on the translocation pathway of nanoparticles across the fetal–maternal barrier of the human placenta suggest that endocytosis plays an important role in the trans-

portation of nanoparticles [12, 15, 32, 38]. In the present study on the mouse placenta, an increase in the number of endocytic vesicles was also observed in the cytoplasm of the syncytiotrophoblasts and fetal endothelial cells by electron microscopy, suggesting that endocytosis was upregulated in the maternal–fetal barrier after administration of gold nanoparticle solutions. Endocytosis plays an important role for the transport of nutrients or biomolecules, such as albumin, folic acid, hormones, etc. at the placenta in the physiological condition [16, 27].

Clathrin-mediated endocytosis was previously described in the cytoplasm of syncytiotrophoblasts of the mouse placenta [16]. Clathrin-mediated endocytosis is involved in the recycling of albumin in the term placenta, neurotransmitter transport and the internalization of several antigens [16, 21, 23]. In this study, clathrin immunohistochemistry showed an increase of intense positivity in the endocytic vesicles of both syncytiotrophoblasts and fetal endothelial cells. The localization of clathrin expression was confirmed by performing double immunofluorescence by using antibodies to clathrin and cytokeratin. Clathrin was also demonstrated in the syncytiotrophoblasts and fetal vascular endothelium. Immunoblot analysis showed an increase in clathrin protein expression in the placental tissues from mice treated with gold nanoparticles. These results suggested that gold nanoparticle administration upregulates clathrin expression in the placenta and that clathrin-mediated endocytosis may be one of the pathways of gold nanoparticle translocation in the maternal–fetal barrier.

Caveolae-mediated endocytosis is also considered to be one of the pathways for the translocation of nanoparticles in the air–blood barrier [26]. Caveolin-1 protein plays a role in the regulation of caveolar invagination and the formation of caveolae, which is one form of the endocytic vesicle [19, 25, 27, 28]. In murine placental tissues, the localization of caveolin-1 has been demonstrated in the vasculatures, especially in the fetal vascular endothelium [3, 20, 22]. In this study, increased intensity of caveolin-1 immunohistochemistry was observed exclusively in the fetal endothelium after the administration of gold nanoparticle solutions. In contrast, immunoblotting showed no difference in the amount of caveolin-1 expression between the control mice and the mice treated with gold nanoparticles, suggesting the possible re-assembly of caveolin-1 protein from the cytosol to the caveolae structure.

In this study with the experimental design, applied techniques including electron microscopy failed to detect signs of actual translocation of the exposed particles as well as signs of their toxicity. However, an increase of endocytic vesicles in the cytoplasm of syncytiotrophoblasts and fetal endothelial cells in the maternal–fetal barrier of mice treated with gold nanoparticles was demonstrated. A further study with prolonged duration, different kinds of nanoparticles and sensitive techniques for the detection of nanoparticles is required to ascertain whether exposed nanoparticles may have a chance to be translocated through the maternal–fetal barrier by both clathrin-mediated and caveolae-mediated endocytosis demonstrated in this study.

ACKNOWLEDGMENTS. This work was supported in part by JSPS KAKENHI Grant Number 24580425 and a Special Project (Assessment and Control of Dust Emission in Degraded Drylands of East Asia), MEXT, Japan for the research, authorship and/or publication of this article. The authors thank Ms. M. Taniguchi at Tottori University for her excellent assistance with electron microscopy and Dr. M. Naota, Ms. Y. Kohara, Mr. Y. Kobayashi and Ms. M. Nemoto for their technical assistance.

REFERENCES

1. Austin, C. A., Umbreit, T. H., Brown, K. M., Barber, D. S., Dair, B. J., Francke-Carroll, S., Feswick, A., Saint-Louis, M. A., Hikawa, H., Siebein, K. N. and Goering, P. L. 2012. Distribution of silver nanoparticles in pregnant mice and developing embryos. *Nanotoxicology* **6**: 912–922. [Medline] [CrossRef]
2. Balasubramanian, S. K., Jittiwat, J., Manikandan, J., Ong, C., Yu, L. E. and Ong, W. 2010. Biodistribution of gold nanoparticles and gene expression changes in the liver and spleen after intravenous administration in rats. *Biomaterials* **31**: 2034–2042. [Medline] [CrossRef]
3. Byrne, S., Ahenkorah, J., Hottor, B., Lockwood, C. and Ockleford, C. D. 2007. Immuno-electron microscopic localization of caveolin 1 in human placenta. *Immunobiology* **212**: 39–46. [Medline] [CrossRef]
4. Buerki-Thurnherr, T., von Mandach, U. and Wick, P. 2012. Knocking at the door of the unborn child: engineered nanoparticles at the human placental barrier. *Swiss. Med. Wkly.* **142**: w13559. [Medline]
5. Cartwright, L., Poulsen, M. S., Nielsen, H. M., Pojana, G., Knudsen, L. E., Saunders, M. and Rytting, E. 2012. *In vitro* placental model optimization for nanoparticle transport studies. *Int. J. Nanomedicine* **7**: 497–510. [Medline]
6. Conner, S. D. and Schmid, S. L. 2003. Regulated portals of entry into the cell. *Nature* **422**: 37–44. [Medline] [CrossRef]
7. Danscher, G. 1984. Autometallography. a new technique for light and electron microscopic visualization of metals in biological tissues (gold, silver, metal sulphides). *Histochemistry* **81**: 331–335. [Medline] [CrossRef]
8. Danscher, G. and Stoltenberg, M. 2006. Silver enhancement of quantum dots resulting from (1) metabolism of toxic metals in animals and humans, (2) *in viv*o, *in vitro* and immersion created zinc-sulphur/zinc-selenium nanocrystals, (3) metal ions liberated from metal implants and particles. *Prog. Histochem. Cytochem.* **41**: 57–139. [Medline] [CrossRef]
9. Elsaesser, A. and Howard, V. 2012. Toxicology of nanoparticles. *Adv. Drug Deliv. Rev.* **64**: 129–137. [Medline] [CrossRef]
10. Ema, M., Kobayashi, N., Naya, M., Hanai, S. and Nakanishi, J. 2010. Reproductive and developmental toxicity studies of manufactured nanomaterials. *Reprod. Toxicol.* **30**: 343–352. [Medline] [CrossRef]
11. Furukawa, S., Hayashi, S., Usuda, K., Abe, M., Hagio, S. and Ogawa, I. 2011. Toxicological pathology in the rat placenta. *J. Toxicol. Pathol.* **24**: 95–111. [Medline] [CrossRef]
12. Keelan, J. A. 2011. Nanoparticles versus the placenta. *Nanotoxicology* **6**: 263–264.
13. Khan, H. M., Khan, M. Y. and Minhas, L. A. 2011. Histological study of the developing mouse placenta. *J. Rawal. Med. Coll.* **15**: 116–119.
14. Kirby, D. R. S. and Bradbury, S. 1965. The hemo-chorial mouse placenta. *Anat. Rec.* **152**: 279–281. [Medline] [CrossRef]

15. Kulvietis, V., Zalgeviciene, V., Didzipetriene, J. and Rotomskis, R. 2011. Transport of nanoparticles through the placental barrier. *Tohoku J. Exp. Med.* **225**: 225–234. [Medline] [CrossRef]
16. Lambot, N., Lybaert, P., Boom, A., Delogne-Desnoeck, J., Vanbellinghen, A. M., Graff, G., Lebrun, P. and Meuris, S. 2006. Evidence for a clathrin-mediated recycling of albumin in human term placenta. *Biol. Reprod.* **75**: 90–97. [Medline] [CrossRef]
17. Lasagna-Reeves, C., Gonzalez-Romero, D., Barria, M. A., Olmedo, I., Clos, A., Ramanujam, V. M. S., Urayama, A., Vergara, L., Kogan, M. J. and Soto, C. 2010. Bioaccumulation and toxicity of gold nanoparticles after repeated administration in mice. *Biochem. Biophys. Res. Commun.* **393**: 649–655. [Medline] [CrossRef]
18. Le Roy, C. and Wrana, J. L. 2005. Clathrin- and non-clathrin-mediated endocytic regulation of cell signalling. *Nat. Rev. Mol. Cell Biol.* **6**: 112–126. [Medline] [CrossRef]
19. Linton, E. A., Rodriguez-Linares, B., Rashid-Doubell, F., Ferguson, D. J. P. and Redman, C. W. G. 2003. Caveolae and caveolin-1 in human term villous trophoblast. *Placenta* **24**: 745–757. [Medline] [CrossRef]
20. Lyden, T. W., Anderson, C. L. and Robinson, J. M. 2002. The endothelium but not the synctiotrophoblast of human placenta expresses caveolae. *Placenta* **23**: 640–652. [Medline] [CrossRef]
21. McMahon, H. T. and Boucrot, E. 2011. Molecular mechanism and physiological functions of clathrin-mediated endocytosis. *Nat. Rev. Mol. Cell Biol.* **12**: 517–533. [Medline] [CrossRef]
22. Mohanty, S., Anderson, C. L. and Robinson, J. M. 2010. The expression of caveolin-1 and the distribution of caveolae in the murine placenta and yolk sac: parallels to the human placenta. *Placenta* **31**: 144–150. [Medline] [CrossRef]
23. Mousavi, S. A., Malerød, L., Berg, T. and Kjeken, R. 2004. Clathrin-dependent endocytosis. *Biochem. J.* **377**: 1–6. [Medline] [CrossRef]
24. Myllynen, P. K., Loughran, M. J., Howard, C. V., Sormunen, R., Walsh, A. A. and Vähäkangas, K. H. 2008. Kinetics of gold nanoparticles in the human placenta. *Reprod. Toxicol.* **26**: 130–137. [Medline] [CrossRef]
25. Nabi, I. R. and Le, P. U. 2003. Caveolae/raft-dependent endocytosis. *J. Cell Biol.* **161**: 673–677. [Medline] [CrossRef]
26. Naota, M., Shimada, A., Morita, T., Yamamoto, Y., Inoue, K. and Takano, H. 2013. Caveolae-mediated endocytosis of intratracheally instilled gold colloid nanoparticles at the air–blood barrier in mice. *Toxicol. Pathol.* **41**: 487–496. [Medline] [CrossRef]
27. Pelkmans, L. and Helenius, A. 2002. Endocytosis via caveolae. *Traffic* **3**: 311–320. [Medline] [CrossRef]
28. Rothberg, K. G., Heuser, J. E., Donzell, W. C., Ying, Y., Glenney, J. R. and Anderson, R. G. W. 1992. Caveolin, a protein component of caveolae membrane coats. *Cell* **68**: 673–682. [Medline] [CrossRef]
29. Sadauskas, E., Danscher, G. and Stoltenberg, M. 2009. Protracted elimination of gold nanoparticles from mouse liver. *Nanomedicine* **5**: 162–169. [Medline]
30. Sadauskas, E., Wallin, H., Stoltenberg, M., Vogel, U., Doering, P., Larsen, A. and Danscher, G. 2007. Kupffer cells are central in the removal of nanoparticles from the organism. *Part. Fibre Toxicol.* **4**: 10. [Medline] [CrossRef]
31. Sadauskas, E., Jacobsen, N. R., Danscher, G., Stoltenberg, M., Vogel, U., Larsen, A., Kreyling, W. and Wallin, H. 2009. Biodistribution of gold nanoparticles in mouse lung following intratracheal instillation. *Chem. Cent. J.* **3**: 16. [Medline] [CrossRef]
32. Saunders, M. 2009. Transplacental transport of nanomaterials. *Wiley Interdiscip. Rev. Nanomed. Nanobiotechnol.* **1**: 671–684. [Medline] [CrossRef]
33. Semmler-Behnke, M., Kreyling, W. G., Lipka, J., Fertsch, S., Wenk, A., Takenaka, S., Schmid, G. and Brandau, W. 2008. Biodistribution of 1.4- and 18-nm gold particles in rats. *Small* **4**: 2108–2111. [Medline] [CrossRef]
34. Shukla, R., Bansal, V., Chaudhary, M., Basu, A., Bhonde, R. R. and Sastry, M. 2005. Biocompatibility of gold nanoparticles and their endocytotic fate inside the cellular compartment: a microscopic overview. *Langmuir* **21**: 10644–10654. [Medline] [CrossRef]
35. Sonavane, G., Tomoda, K. and Makino, K. 2008. Biodistribution of colloidal gold nanoparticles after intravenous administration: effect of particle size. *Colloids Surf. B Biointerfaces* **66**: 274–280. [Medline] [CrossRef]
36. Sung, J. H., Ji, J. H., Park, J. D., Song, M. Y., Song, K. S., Ryu, H. R., Yoon, J. U., Jeon, K. S., Jeong, J., Han, B. S., Chung, Y. H., Chang, H. K., Lee, J. H., Kim, D. W., Kelman, B. J. and Yu, I. J. 2011. Subchronic inhalation toxicity of gold nanoparticles. *Part. Fibre Toxicol.* **8**: 16. [Medline] [CrossRef]
37. Takata, K., Fujikura, K. and Shin, B. 1997. Ultrastructure of the rodent placental labyrinth: a site of barrier and transport. *J. Reprod. Dev.* **43**: 13–24. [CrossRef]
38. Wick, P., Malek, A., Manser, P., Meili, D., Maeder-Althaus, X., Diener, L., Diener, P., Zisch, A., Krug, H. F. and von Mandach, U. 2010. Barrier capacity of human placenta for nanosized materials. *Environ. Health Perspect.* **118**: 432–436. [Medline] [CrossRef]
39. Yamashita, K., Yoshioka, Y., Higashisaka, K., Mimura, K., Morishita, Y., Nozaki, M., Yoshida, T., Ogura, T., Nabeshi, H., Nagano, K., Abe, Y., Kamada, H., Monobe, Y., Imazawa, T., Aoshima, H., Shishido, K., Kawai, Y., Mayumi, T., Tsunoda, S., Itoh, N., Yoshikawa, T., Yanagihara, I., Saito, S. and Tsutsumi, Y. 2011. Silica and titanium dioxide nanoparticles cause pregnancy complications in mice. *Nat. Nanotechnol.* **6**: 321–328. [Medline] [CrossRef]
40. Yang, W., Peters, J. I. and Williams, R. O. III. 2008. Inhaled nanoparticles–a current review. *Int. J. Pharm.* **356**: 239–247. [Medline] [CrossRef]